Metodi Numerici per la Fisica

Anno accademico 2022/2023

Fabio Marinello
January 19, 2024

Contents

Module 1

Thermodynamics of the 2D Ising model via Markov chain Monte Carlo methods

1.1 The Ising model

Let us consider an $L \times L$ lattice where each site is occupied by a binary spin variable $s \in \{\pm 1\}$. We suppose that each spin interacts only with its nearest neighbours with interaction strength J, and that there is an external local magnetic field h: the Hamiltonian of the system is thus

$$H[\boldsymbol{\sigma}] = -J \sum_{\langle i,j \rangle} s_i s_j - h \sum_i s_i \tag{1.1}$$

for a given configuration $\boldsymbol{\sigma}$ of all spins occurring with probability given by the Gibbs distribution

$$P[\boldsymbol{\sigma}] = \frac{\exp(-\beta H[\boldsymbol{\sigma}])}{Z}, \quad \text{where } Z = \sum_{\{\boldsymbol{\sigma}\}} \exp(-\beta H[\boldsymbol{\sigma}]). \tag{1.2}$$

For simplicity, we will consider a ferromagnetic ($J > 0$) model with $J = 1$ and no external field $h = 0$; furthermore, we fix $k_B = 1$ so that β is simply the inverse temperature $1/T$. Finally, we set periodic boundary conditions so that each site has exactly four neighbours.

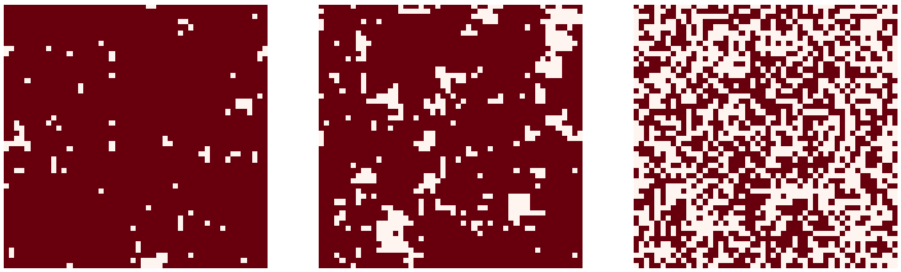

Figure 1.1: The variable β is the *control parameter* of the system and determines its level of order: at lower temperatures (left), the spins of the lattice will tend to be mostly aligned with each other in a configuration of low energy, while at higher temperature (right) the increasing statistical fluctuations will make the system more and more random. At the critical beta (middle), the (infinite) lattice is self-similar: no matter how far or near we look at it, the distribution of the spin clusters will look the same.

1.2 The Metropolis-Hastings algorithm

In order to study the thermodynamical observables of the system, we need to compute their averages over a large number of lattices. Thus, we need a way to generate them according to the correct probability distribution. One way of achieving this is by employing a Markov chain Monte Carlo (MCMC) method known as the *Metropolis-Hastings* algorithm, which works as follows.

Consider the space $\Sigma = \{\boldsymbol{\sigma}\}$ of all possible configurations of the system. Starting from a configuration $\boldsymbol{\sigma}_0 \in \Sigma$, our goal is to build a path $(\boldsymbol{\sigma}_0, \boldsymbol{\sigma}_1, \boldsymbol{\sigma}_2, ...)$ in Σ such that each configuration $\boldsymbol{\sigma}_k$ for large enough k is reached with probability given by $P[\boldsymbol{\sigma}_k]$. The time it takes for the chain to reach this equilibrium state is known as *thermalization*, and we will need to take it into account when performing the simulation.

In order to accomplish this, we need to write down the transition probability $W(\boldsymbol{\sigma} \to \boldsymbol{\sigma}')$ from one configuration to the next, which is given by the product of the selection probability S and the rate of acceptance A:

$$W(\boldsymbol{\sigma} \to \boldsymbol{\sigma}') = S(\boldsymbol{\sigma} \to \boldsymbol{\sigma}')A(\boldsymbol{\sigma} \to \boldsymbol{\sigma}'). \tag{1.3}$$

The easiest possibility for the transition $\boldsymbol{\sigma} \to \boldsymbol{\sigma}'$ is to select a random spin and invert it: since this is done with uniform probability, $S(\boldsymbol{\sigma} \to \boldsymbol{\sigma}') = 1/L^2$. The configuration $\boldsymbol{\sigma}'$ is only accepted if it takes us closer to our goal of realizing a Boltzmann distribution: thus, the Metropolis-Hasting rule requires an acceptance rate

$$A(\boldsymbol{\sigma} \to \boldsymbol{\sigma}') = \begin{cases} \exp\left[\beta(E[\boldsymbol{\sigma}'] - E[\boldsymbol{\sigma}])\right] & \text{if } E[\boldsymbol{\sigma}'] - E[\boldsymbol{\sigma}] > 0, \\ 1 & \text{otherwise.} \end{cases} \tag{1.4}$$

The detailed balanced condition therefore gives

$$\frac{W(\boldsymbol{\sigma} \to \boldsymbol{\sigma}')}{W(\boldsymbol{\sigma}' \to \boldsymbol{\sigma})} = \frac{A(\boldsymbol{\sigma} \to \boldsymbol{\sigma}')}{A(\boldsymbol{\sigma}' \to \boldsymbol{\sigma})} = \frac{P(\boldsymbol{\sigma}')}{P(\boldsymbol{\sigma})} = \exp[-\beta(E[\boldsymbol{\sigma}'] - E[\boldsymbol{\sigma}])]. \tag{1.5}$$

We note that in order to compute the energy difference $\Delta E[\boldsymbol{\sigma}, \boldsymbol{\sigma}']$ between the original and candidate configurations, there is no need to find the individual total energies: in fact, since only one site i_0 is modified, we have

$$\Delta E = 2 s_{i_0} S[i_0], \tag{1.6}$$

where $S[i_0]$ is the sum over the neighbour spins of i_0. This observation will allow us to make our code a lot more efficient.

1.3 Thermodynamic observables

Given a probability distribution $p(x)$, the average of a function $f(x)$ is generally computed as $\langle f \rangle = \int p(x) f(x) dx$; in Monte Carlo simulations this is replaced by the sample mean $\bar{f} = \frac{1}{N} \sum_i f_i$, where f_i are N data points distributed according to $p(x)$.

During our simulation of the Ising model, we compute in this way the two fundamental quantities of interest, the average energy per spin

$$\langle \varepsilon \rangle = \frac{\langle E \rangle}{L^2}, \tag{1.7}$$

and the average magnetization per spin

$$\langle m \rangle = \frac{\langle M \rangle}{L^2} = \frac{1}{L^2} \sum_i s_i. \tag{1.8}$$

To check that the system is evolving correctly under this algorithm, we can take a look at the Monte Carlo histories of these quantities and check that the values are consistent with our expectations.

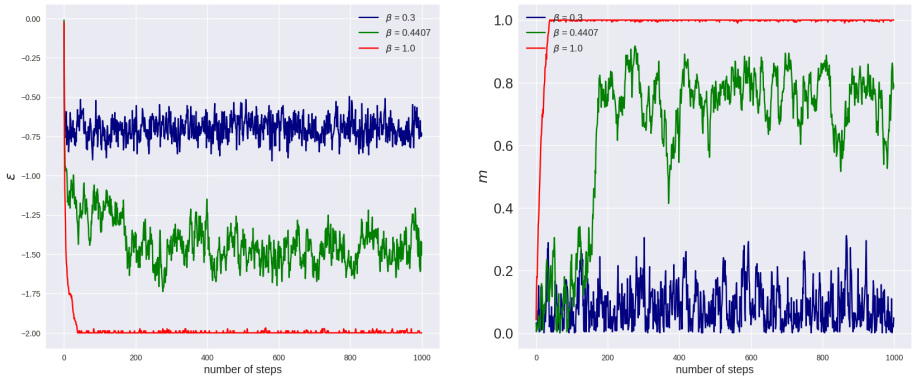

Figure 1.2: Monte Carlo histories of ε and m for various values of β.

Then, we may compute the specific heat and the magnetic susceptibility respectively as the variance of the energy and the magnetization:

$$C = \beta^2 L^2(\langle \varepsilon^2 \rangle - \langle \varepsilon \rangle^2), \quad \chi = \beta L^2(\langle m^2 \rangle - \langle m \rangle^2). \tag{1.9}$$

The average magnetization is a particularly interesting quantity, as it can be shown that there exists a critical value $\beta_c \approx 0.4407$ for which the system undergoes a phase transition from a disordered, paramagnetic phase where $\langle m \rangle = 0$ to an ordered, ferromagnetic one where $\langle M \rangle \neq 0$. Correspondingly, the average energy will vary from zero in the disordered phase, to the minimum value ± 2 for a completely ordered one.

In his famous analytic solution of the 2D Ising model, Onsanger was able to find for $T_c = 1/\beta_c$ the closed expression

$$T_c = \frac{2}{\ln(1+\sqrt{2})} \approx 2.27. \tag{1.10}$$

Even if we are only capable of simulating systems with finite size and therefore unable to see actual divergences around this critical point, we can still see from the graph below that the value of the magnetic susceptibility χ (a second derivative of the free energy) increases dramatically with L as the critical point is approached, showing that a second order phase transition is happening at T_c.

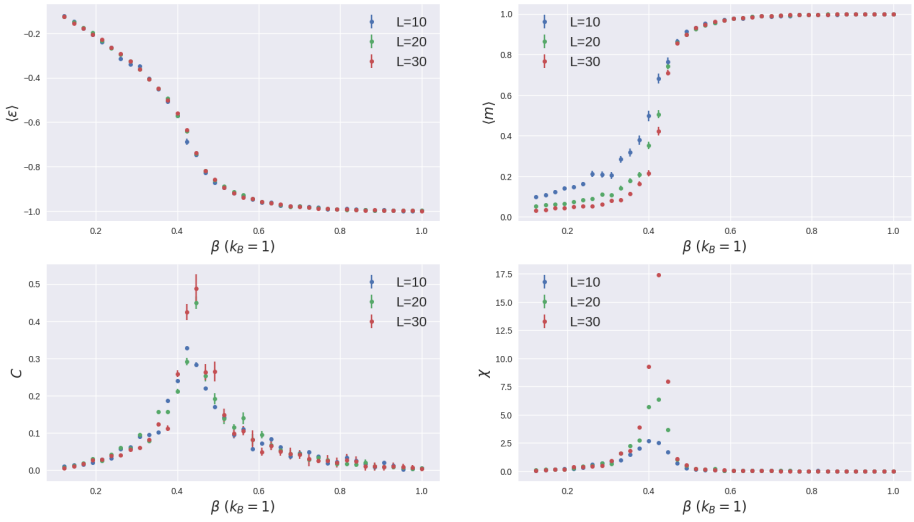

Figure 1.3: $\langle \varepsilon \rangle$, $\langle m \rangle$, C and χ for $\beta \in [0, 1]$ and three lattice sizes $L = 10, 20, 30$.

A note on error analysis

Our strategy to only change a single spin when going from one configuration to the next has the advantage of simplicity, but also a significant drawback: the naive error estimate

$$\sigma_f^2 = \frac{N}{N-1}\langle (f - \langle f \rangle_p)^2 \rangle_p \tag{1.11}$$

is inaccurate, as we need to take the strong correlation within neighbouring data points into account.

We may proceed in two ways to get rid of this issue. The first is to simply measure our quantities only for a subset of the generated lattices, for instance every thirty or forty Metropolis steps. This will ensure that enough random changes have occurred in the starting configuration to eliminate most of the correlation, although longer simulations are required to collect the same amount of data. The second is to implement decorrelation techniques such as *blocking* algorithms, the *bootstrap*, or the *jacknife*.

In particular, for complicated estimators such as the specific heat and the magnetic susceptibility we have employed the bootstrap algorithm, which roughly works as follows: build new samples from the original one using random blocks of data points (allowing multiple extractions of the same elements) and compute the average of each new sample. At the end, the variance of the averages should be a better estimate of the true error.

1.4 Ergodicity

A system is said to be *ergodic* in a certain regime if it is able to explore the entire configuration space Σ through the simulation. In the case of the Ising model, the system is ergodic for $\beta < \beta_c$, but this property is lost above the critical point. This is due to the fact that the free energy f behaves differently depending on the temperature: for $\beta < \beta_c$, f has a minimum at $m = 0$, for $\beta = \beta_c$ it has two coinciding minima at $m = 0$, and finally for $\beta > \beta_c$ it has two different minima at $\pm\bar{m}$.

Concretely, we may plot the histogram of the magnetizations computed with respect to the generated lattices. Depending on the value of β, the graph will be shaped differently: below β_c it will look like a Gaussian distribution centered on $m = 0$, more and more approaching a Dirac delta $\delta(0)$ as L becomes larger, while above β_c, it will show two peaks centered at ± 1 respectively. This is because as β increases there are fewer and fewer configurations with $\langle M \rangle = 0$, acting as a sort of barrier between the two possibilities $\langle M \rangle = \pm 1$ and causing *ergodicity breaking*.

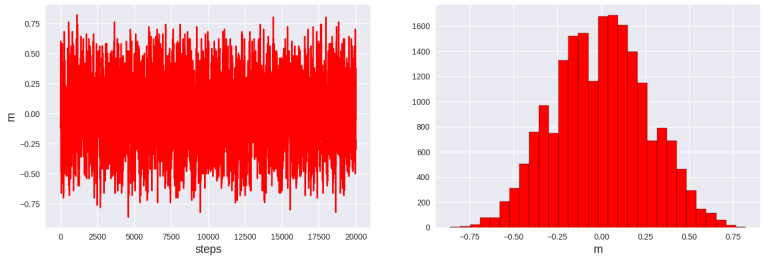

Figure 1.4: distribution in the disordered phase at $T > T_c$.

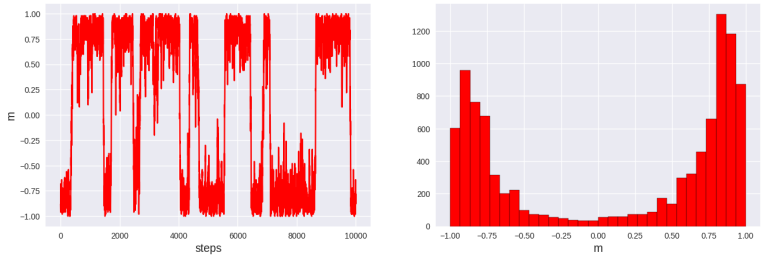

Figure 1.5: distribution at the critical temperature $T = T_c$.

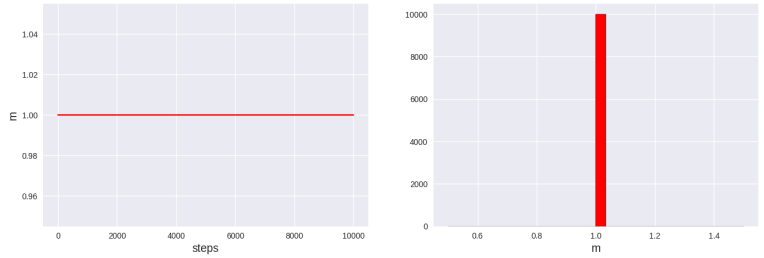

Figure 1.6: distribution in the ordered phase at $T < T_c$.

1.5 Critical exponents

Around the critical point, the correlation length ξ of the system diverges and the thermodyamical observables behave according to power laws with universal critical exponents: defining $t = \frac{T - T_c}{T_c}$, we have

$$\xi \sim |t|^{-\nu}, \quad \langle M \rangle \sim |t|^{\beta}, \quad \chi \sim |t|^{-\gamma}, \quad C \sim |t|^{-\alpha} \tag{1.12}$$

where $\alpha = 0$, $\beta = \frac{1}{8}$, $\gamma = \frac{7}{4}$ and $\nu = 1$. We should keep in mind that for systems that are finite in size the correlation length cannot diverge, and therefore we should expect some differences between the theoretical, $N \to +\infty$ values of β_c and of the critical exponents and the results of our numerical simulations; nevertheless, we proceed to determine as an example the value of χ with a power law fitting function.

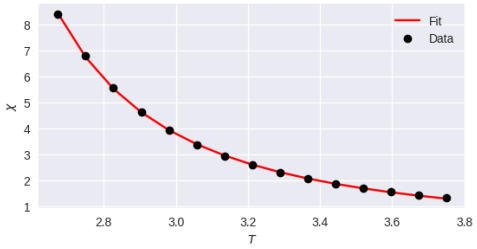

Figure 1.7: fitting the magnetic susceptibility χ at size $L = 30$ with a power law of the form $K|T - T_c|^{\gamma}$, we find values that are in reasonable agreement with the theory.

par	value	δ
γ	-1.739	± 0.002
K	3.08	± 0.01

Once the critical exponents have been found, it is possible to verify that around the critical point the thermodynamical observables follow the *finite scaling ansatz*: given the scaling functions ϕ_M, ϕ_χ we have the relations

$$\chi \sim L^{\gamma/\nu}\tilde{\phi}_\chi[(\beta - \beta_c)L^{1/\nu}], \quad \langle |M| \rangle \sim L^{-\beta/\nu}\phi_M[(\beta - \beta_c)L^{1/\nu}]. \tag{1.13}$$

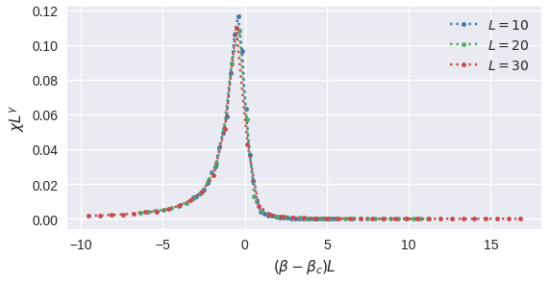

Figure 1.8: the shape of the ϕ_χ function, obtained plotting $\chi L^{7/4}$ against the variable $(\beta - \beta_c)L$, remains the same regardless of the size of the system.

1.6 The Wolff algorithm

As we mentioned above, one issue with the standard single-flip Metropolis algorithm is that the correlation function

$$C_2(\tau) = \frac{\langle (x_t - \langle x \rangle)(x_{t+\tau} - \langle x \rangle) \rangle}{\langle (x_t - \langle x \rangle)^2 \rangle} \tag{1.14}$$

becomes very large around the critical point, making the simulation particularly inefficient right at the place where most of the physics is happening: this is a phenomenon known as *critical slowing down*.

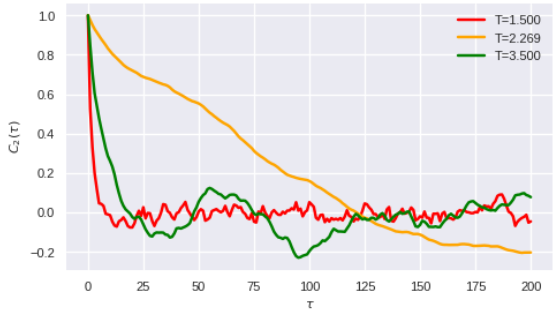

Figure 1.9: at the critical temperature, each flip is felt at a much larger distance than at lower or higher temperatures, hence the self-similar nature of the lattice and the power law behaviour of β-dependent quantities.

In order to fix this, we can make a slight modification to the algorithm so that at each iteration several clustered spins are flipped at the same time; this is known as the *Wolff algorithm*. Informally, the algorithm goes as follows:

1. Pick a random spin s and remember its direction; this is the first element of the cluster.
2. For each neighbouring spin that is also aligned with σ, add it to the cluster with probability $1 - e^{-2J\beta}$.
3. Repeat the second step for each newly added spin; when no more spins are added, flip the whole cluster.

More formally, if $J = 1$ the transition probability is now given by

$$W(\boldsymbol{\sigma} \to \boldsymbol{\sigma}') = \min\left(1, \frac{e^{-\beta(n-m)}}{(1-p)^n} \frac{(1-p)^m}{e^{-\beta(m-n)}}\right), \quad p = 1 - e^{-2\beta}, \tag{1.15}$$

where p represents the probability of adding an aligned neighbouring spin to the cluster, n is the number of aligned spins that are not accepted, and m is the number of aligned spins near the cluster after the flipping process.

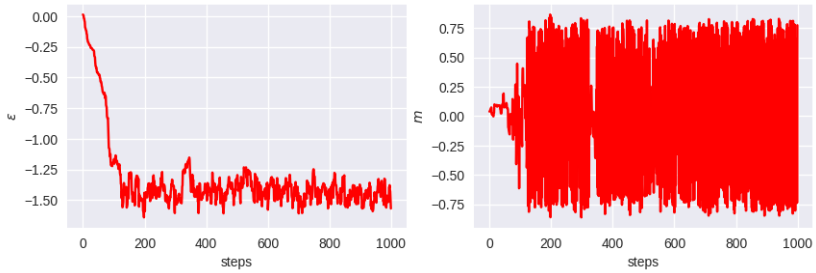

Figure 1.10: Monte Carlo histories of the energies and magnetizations computed at β_c with the Wolff algorithm. While the energy graph looks essentially the same as the one in figure 2, the magnetization oscillates much faster as the system changes state much more quickly.

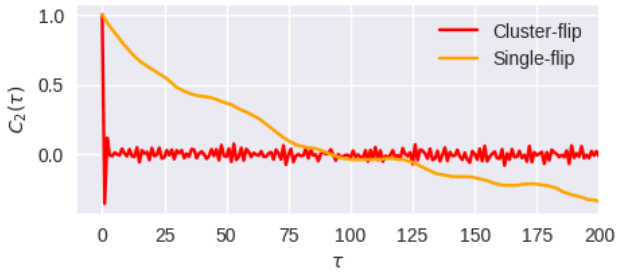

Figure 1.11: the advantage of the Wolff algorithm over the standard single spin-flip algorithm is evident from this plot, a comparison between the correlation function of both algorithms at T_c.

Module 2

Exact diagonalization of the quantum Ising spin chain

2.1 The quantum Ising model

Let us consider a chain of N spin-$\frac{1}{2}$ particles with nearest neighbour interactions along the $\hat{z}$ axis as well as an external transverse magnetic field: the Hamiltonian of such system is

$$\hat{H} = -J \sum_j \hat{\sigma}_j^z \hat{\sigma}_{j+1}^z - h \sum_j \hat{\sigma}_j^x. \tag{2.1}$$

This is a simple instance of the more general quantum Ising model with arbitrary interactions on a d-dimensional lattice, useful in statistical mechanics for the study of ferromagnetic materials. In the following, we will either consider open boundary conditions (i.e., the leftmost and rightmost spins do not interact with each other) or periodic boundary conditions and set for simplicity $J = 1$.

Dispersion law. The description of the Hamiltonian in terms of the local Pauli matrices $\hat{\sigma}_j^z$, $\hat{\sigma}_j^x$ may be derived from the natural ladder-operator formalism by employing the so-called *Jordan-Wigner transformation* on the expression

$$\hat{H} = -J \sum_j \left\{ (\hat{c}_j^\dagger \hat{c}_{j+1} + \hat{c}_{j+1}^\dagger \hat{c}_j) + \hat{c}_j^\dagger \hat{c}_{j+1}^\dagger + \hat{c}_{j+1} \hat{c}_j) \right\} - 2h \sum_j \left(\hat{c}_j^\dagger \hat{c}_j - \frac{1}{2} \right).$$

Introducing the fermionic Bogoliubov operators, the Hamiltonian can be written in the simple diagonal form

$$\hat{\tilde{H}} = 2 \sum_k \epsilon_k \left(\hat{b}_k^\dagger \hat{b}_k - \frac{1}{2} \right) \tag{2.2}$$

and assuming a uniform external field it is possible to find the explicit expression for the energy levels

$$\varepsilon_k = \sqrt{1 + \frac{h^2}{J^2} + \frac{2h}{J}\cos\left(\frac{2\pi k}{N}\right)}, \tag{2.3}$$

for $k \in \left[-\frac{N}{2} + 1, ..., \frac{N}{2}\right]$.

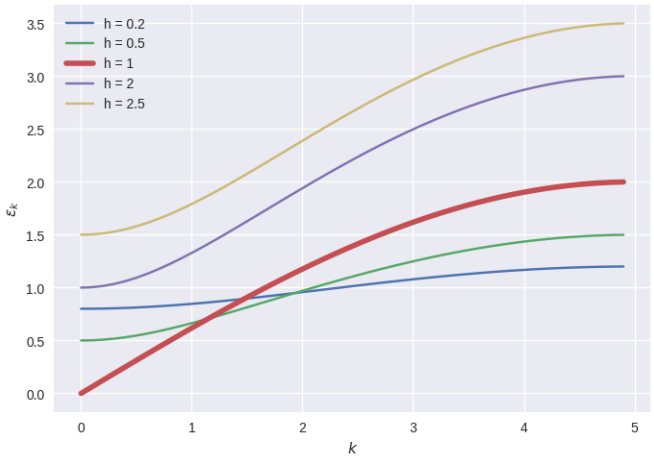

Figure 2.1: the different shapes of the curves for $h = 1$ and $h \neq 1$.

From the graph we see that the system is gapless for $h = 1$, but gapped for all other values. This suggests that the ground state of the system exhibits a quantum phase transition at the critical Ising point $h = 1$ where it goes from a disordered paramagnetic phase to an ordered ferromagnetic one.

Integrability and level crossing. Using the dispersion relation as well as the exact diagonalization methods discussed below, it is possible to show that the Ising model is integrable. While the normalized energy gaps

$$\frac{\delta E_j}{\langle \delta E_j \rangle}, \quad j = 1, \dots, 2^N \tag{2.4}$$

are never zero for non-integrable systems and follow the *Wigner-Dyson* statistics $P(s) \sim s^\gamma e^{-s^2}$ (where $\gamma > 0$) characterized by a global maximum around $s = 1$, integrable systems exhibit the phenomenon of *level crossing* and a thickening of gap counts near $s = 0$, implying a large degree of degeneration.

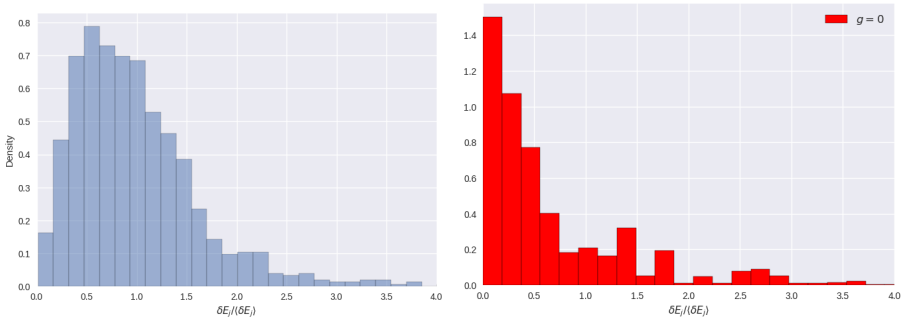

Figure 2.2: renormalized energy gaps for an integrable (right) and non-integrable (left) Ising models. The energies have been calculated with the methods described in the following section.

2.2 Exact diagonalization

In order to find the energy levels of the Ising system numerically, we follow the technique of exact diagonalization: given the Hamiltonian H, we construct the associated basis and employ an algorithm such as the Lanczos algorithm that is able to compute the ground state energy and the corresponding eigenstate. To find the full spectrum, we have made use of the *scipy.linalg* library as a wrapper of LAPACK, a Fortran library that contains eigenvalue-finding subroutines such as *dgeev*.

Exact diagonalization is straightforward, but inefficient due to the sheer size of the Hilbert space, which grows exponentially with the number of spins in the chain. Luckily, noticeable improvements can be made by noticing that the Hamiltonian matrix for large N is sparse, that is, the vast majority of its entries are null. This allows us to store only its non-zero entries along with their coordinates, saving up precious memory for our computations.

In order to check the validity of our methods, we plot the ground state energy for various values of N when $h = 1$, which should follow the curve given by

$$E_0(N) = 1 - \left[\sin\left(\frac{\pi}{2(2N+1)}\right)\right]^{-1}. \tag{2.5}$$

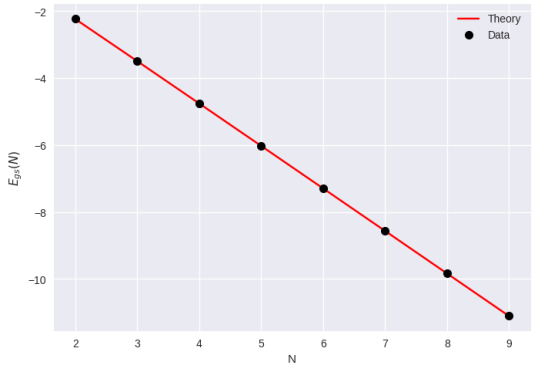

Figure 2.3: ground state energy as a function of N; we find good agreement between the data and the theoretical expectation.

The graphs of the energy gaps between the ground state and the first and second excited states reveal an interesting feature of the model. While our numerical findings for the splitting $E_2 - E_0$ as a function of the external field h agree with the naive theoretical prediction for all values of h, the gap $E_1 - E_0$ is only in agreement in the range $h > 1$. This means that for $h < 1$ the ground state is degenerate, a feature that is due to one important symmetry of the system: given the operator $\hat{P}_z = \prod_j \hat{\sigma}_j^x$ that inverts all spins with respect to the z-axis, one finds that $[\hat{H}, \hat{P}_z] = 0$. Therefore, whenever a state $|\psi\rangle = \sum_n c_n |n\rangle$ written in the computational basis $\{|n\rangle\}$ is an eigenstate of H, then the state $|\bar{\psi}\rangle = \hat{P}_z |\psi\rangle$ with all spins inverted is also an eigenstate.

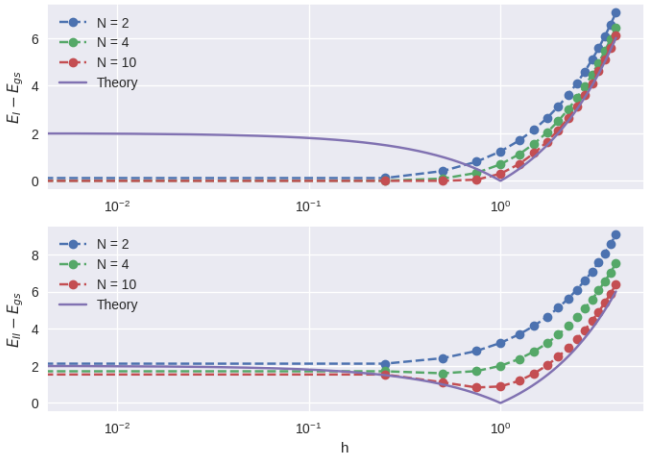

Figure 2.4: first two energy gaps for various chain sizes in logarithmic scale.

2.3 Magnetization

Beside the energy levels, the average magnetization along the z-axis $\langle \hat{M}_z \rangle$ where $\hat{M}_z = \sum_j \hat{\sigma}_j^z$ is the most relevant quantity to our study of the quantum Ising model. We have seen how the transverse field h determines a phase transition between a paramagnet and a ferromagnet; now we will see how the average magnetization is the order parameter of such transition.

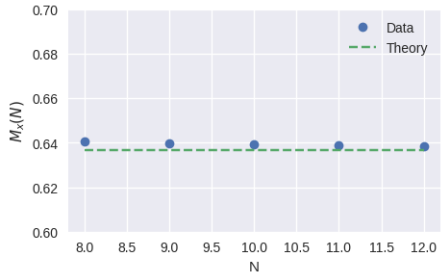

Figure 2.5: the average magnetization along the x-axis is another quantity of interest; in the thermodynamic limit, its value at the critical point is constant at $\langle \hat{M}^x \rangle = 2/\pi$ for every N.

Magnetization and symmetry. Since the ground state in which we wish to compute the average magnetization is doubly degenerate, we need a strategy to make sure that we are computing this quantity effectively. If $|\psi\rangle = \sum_n c_n |n\rangle$ and $|\bar{\psi}\rangle = \sum_n c_n |\bar{n}\rangle$ are the groundstate eigenkets, then the average magnetization in their symmetric and antisymmetric combinations $|\psi_{S,A}\rangle = \frac{1}{\sqrt{2}}(|\psi_1\rangle \pm |\psi_2\rangle)$ is zero, and at finite N these are always found to be the lowest energy eigenstates.

There are a couple ways to break the $\hat{P}_z$ symmetry and avoid this trap. The more cumbersome one (although interesting in its own right) would require the introduction of a longitudinal field g that gets rid of the degeneracy, so that the Hamiltonian becomes

$$\hat{H} = -J \sum_j \hat{\sigma}_j^z \hat{\sigma}_{j+1}^z - h \sum_j \hat{\sigma}_j^x - g \sum_j \hat{\sigma}_j^z; \tag{2.6}$$

the easier approach is computing for any state $|\phi\rangle = \sum_n d_n |n\rangle$ the quantity

$$\langle \hat{\tilde{M}}^z \rangle = \sum_n |d_n|^2 \Big| \sum_j \langle n | \hat{\sigma}_j^z | n \rangle \Big| \tag{2.7}$$

which is insensitive to the direction of the spins along the z-axis.

Choosing the latter route, we calculate the average magnetization for systems of various sizes, plotting the results in logarithmic scale. Together with it, we also report the results for the magnetization along the x-axis, which is computed in an analogous way (though free of the symmetry issue), and the magnetization along $\hat{z}$ as a function of the longitudinal field g when $h = 1$.

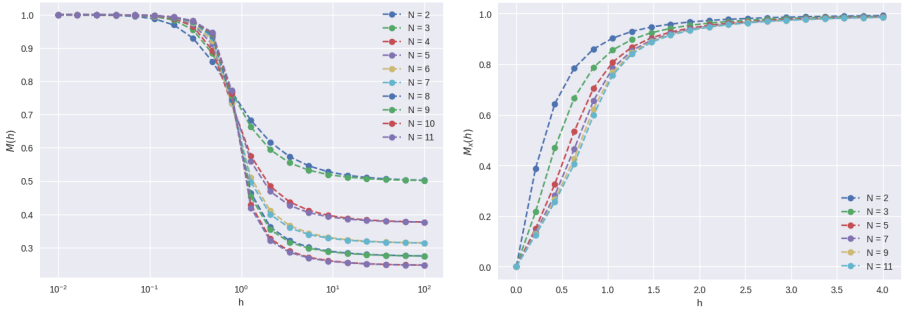

Figure 2.6: plots for different system sizes of the average magnetizations along the $\hat{z}$ and $\hat{x}$ axes.

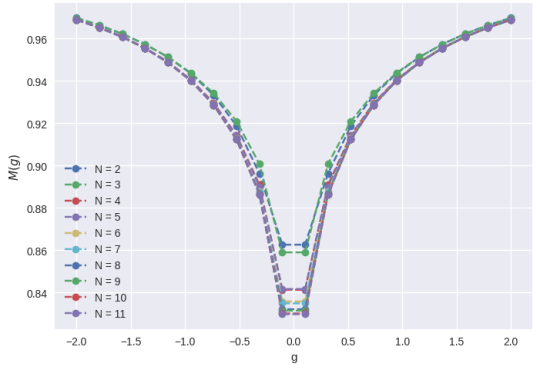

Figure 2.7: magnetization as a function of g for various system sizes at fixed $h = 1$.

As expected, we find that around the critical point at $h = 1$ the system goes from a configuration with $\langle \hat{M}^z \rangle = 0$ to a magnetized one where $\langle \hat{M}^z \rangle \neq 0$. Unlike the case of the 2D classical Ising model, this transition is purely quantum in nature, as we have never abandoned our assumption of zero temperature.

2.4 Response functions

Other quantities of interest for our study of the system are the magnetic susceptibility and the specific heat, defined as the derivatives

$$\chi = \frac{\partial \langle \hat{M}^z \rangle}{\partial h}, \quad C = \frac{\partial \langle E \rangle}{\partial h}. \tag{2.8}$$

The plot of $\chi(h)$ shows a peak at $h = 1$ that becomes more and more pronounced as the size of the system grows, further confirming the presence of a second-order phase transition due to the change in the magnetization; the graph of $C(h)$ shows no such peak, as the energy is not an order parameter for the system, and there are therefore no singular points even in the thermodynamic limit.

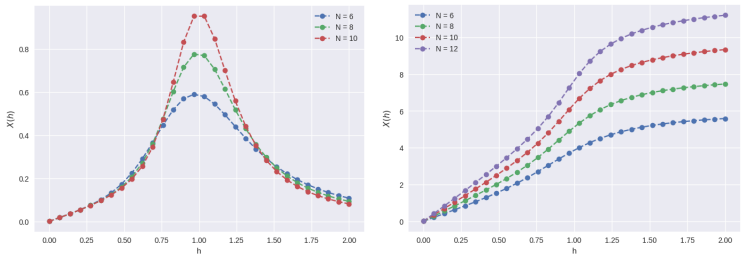

Figure 2.8: magnetic susceptibility and specific heat for various sizes, with the expected peak (and lack thereof) at the critical point.

2.5 Scaling laws

Due to the divergence of the correlation length ξ of the system, at the critical point $(h = 1, g = 0)$ the thermodynamical observables behave according to power laws regulated by universal critical exponents. These exponents, according to the classical-quantum mapping, are the same as the two-dimensional classical Ising model discussed in the first module. For finite dimensional systems, we will need to exchange the correlation length for the size N.

In particular, given the scaling functions ϕ_M, ϕ'_M we have for the average magnetization

$$\langle \hat{M}^z(h, N) \rangle \sim N^{-\beta/\nu} \phi_M(|h - 1| N^{1/\nu}) \tag{2.9}$$

where $\beta = \frac{1}{8}$ and $\nu = 1$, while as a function of the longitudinal field g we have

$$\langle \hat{M}^z(g, N) \rangle \sim N^{-\beta/\nu} \phi'_M(|g - 1| N^{15/8}). \tag{2.10}$$

By rescaling both the independent and dependent variables with the appropriate power of N, we should thus get *data collapse* into a curve that is the same for all sizes of the system, as we can verify by inspecting the following plots.

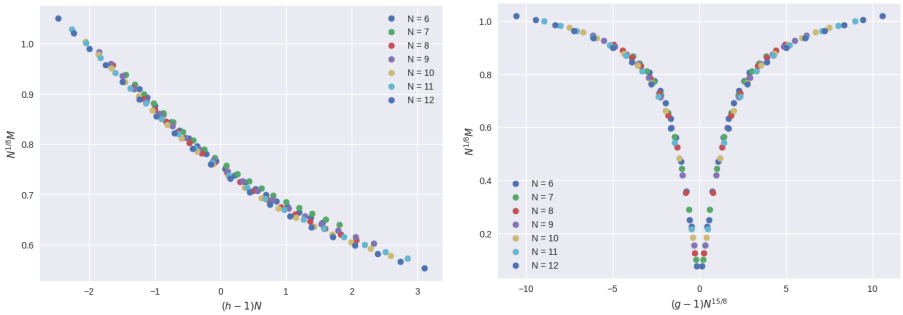

Figure 2.9: scaling laws for the average magnetization along the z-axis as a function of h (left) and g (right).

Module 3

Numerical path integral techniques for the quantum harmonic oscillator

3.1 Averages by path integration

Let $\hat{H}$ be the Hamiltonian of a quantum system, and $\{|n\rangle\}$ the collection of its discrete eigenstates such that $\hat{H}|n\rangle = E_n|n\rangle$. At thermal equilibrium at inverse temperature β, the average value of any observable $\hat{O}$ may be computed as

$$\langle \hat{O} \rangle_\beta = \frac{\mathrm{tr}[\hat{O}e^{-\beta\hat{H}}]}{\mathrm{tr}[e^{-\beta\hat{H}}]} = \sum_n p_n O_n \tag{3.1}$$

where $O_n = \langle n|\hat{O}|n\rangle$ and the probabilistic weight p_n is defined in terms of the partition function $Z = \sum_n e^{-\beta E_n}$ as

$$p_n = \frac{e^{-\beta E_n}}{Z}. \tag{3.2}$$

which is exactly the same as the Gibbs distribution of the microstates that we encountered in the first module.

In order to compute these average values, we might look into performing a Monte Carlo simulation sampling directly from this probability distribution. However, there are some issues with this method: above all, we generally do not know all the eigenvectors and eigenvalues of the system, and therefore O_n is unknown.

In this work, we follow the approach of *path integration*, switching from the energy basis to the computational basis $\{|x\rangle\}$ of the position eigenstates where the partition function becomes

$$Z = \int dx \langle x|e^{-\beta\hat{H}}|x\rangle \tag{3.3}$$

for a Hamiltonian $\hat{H} = \frac{\hat{p}^2}{2m} + V(\hat{q})$. At the heart of the derivation (which is out of the scope of this report) lies the idea of discretizing time into N intervals, which can be achieved via a Trotter decomposition $e^{-\beta\hat{H}} = (e^{-\hat{H}\delta\tau/\hbar})^N$ where $\delta\tau = \beta\hbar/N$. This looks like a standard unitary propagator provided that the substitution $\delta t \to -i\delta\tau$ (known as a *Wick rotation*) is made: each of these N operators is then sandwiched between intermediate states $\langle x_{j+1}|$ and $|x_j\rangle$, for all $j = 1, ..., N-1$, and the BCH formula is used to deal with the kinetic and potential terms separately.

Following this recipe, we obtain in the limit $N \to +\infty$ the fundamental result

$$Z = \mathcal{N} \int Dx(\tau) \exp\left(\frac{S_E[x(\tau)]}{\hbar}\right), \tag{3.4}$$

where $\mathcal{N}$ is a diverging constant, S_E is the Euclidean action

$$S_E = \int_0^{\beta\hbar} d\tau \left(\frac{1}{2}m\dot{x}^2 + V(x)\right) \tag{3.5}$$

and the functional integration is performed over all paths that close on themselves at Euclidean time $\tau = \beta\hbar$. Using the partition function we can compute the average value of any observable as the quantity

$$\langle\hat{O}\rangle_\beta = \frac{1}{Z}\int Dx(\tau) e^{-\frac{S_E[x(\tau)]}{\hbar}} O[x(\tau)] \tag{3.6}$$

which defines the probability distribution of reference for our Monte Carlo simulations

$$P[x(\tau)] = \frac{e^{-\frac{S_E[x(\tau)]}{\hbar}}}{Z}. \tag{3.7}$$

3.2 Application to the harmonic oscillator

The final result of the first section applies to the numerically infeasible limit where $N \to +\infty$. In order to simulate a system such as the harmonic oscillator, characterized by the potential $V(\hat{q}) = \frac{1}{2}m\omega^2\hat{q}^2$, we will use the discrete form

$$\frac{S_{E,L}}{\hbar} = \frac{1}{\hbar}\sum_{j=1}^{N} \delta\tau \left[\frac{1}{2}m\frac{(x_{j+1} - x_j)^2}{(\delta\tau)^2} + \frac{1}{2}m\omega^2 x_j^2\right] \tag{3.8}$$

with periodic boundary conditions $N\delta\tau = \beta\hbar$, $x_{N+1} = x_1$. We also rescale the variables x_j to obtain the adimensional quantities $y_j = \sqrt{\frac{m\omega}{\hbar}}x_j$ in terms of which the action becomes

$$\frac{S_{E,L}}{\hbar} = \sum_{j=1}^{N}\left(\frac{1}{2\eta}(y_{j+1} - y_j)^2 + \frac{\eta}{2}y_j^2\right), \quad \eta = \omega\delta\tau. \tag{3.9}$$

Armed with the discrete action, we are ready to perform a Monte Carlo simulation to sample from the distribution defined by

$$P(y_1, ..., y_N) \propto \exp\left[\sum_{j=1}^{N}\left(\frac{1}{2\eta}(y_{j+1} - y_j)^2 + \frac{\eta}{2}y_j^2\right)\right] \tag{3.10}$$

employing the same Metropolis algorithm that we used in the first module. The selection probability is still the uniform choice of a random path point y_j; a modification $y^p \leftarrow [y_j - \delta, y_j + \delta]$ is then proposed and accepted with probability $r = e^{-\Delta S_{E,L}}$, where the variation of the action may be simplified as

$$\Delta S_{E,L} = \left(\frac{1}{\eta} + \frac{\eta}{2}\right)((y^p)^2 - y^2) + \frac{1}{\eta}(y_j - y^p)(y_{j+1} + y_{j-1}). \tag{3.11}$$

Again, since this algorithm is local and only one point of the discretized path is modified at each step, the correlation in the obtained data will need to addressed in the analysis, either by only measuring after an appropriate number of decorrelation steps or by the use of blocking and bootstrap algorithms.

We briefly describe the blocking method used to compute the error in the internal energy introduced in the next section. The original sample of size N is divided into blocks of size L, and for each block the mean and the variance are computed; the total variance is the sum of each individual block's variance, and the size L is then increased until the statistical error saturates.

3.3 Internal energy

From the theory, we know that the harmonic oscillator has internal energy

$$U = \frac{\partial}{\partial\beta}\log Z = \hbar\omega\left(\frac{1}{2} + \frac{1}{e^{-\beta\hbar\omega} - 1}\right). \tag{3.12}$$

In the path integral formulation, we make use of the discretized version of Z to obtain

$$U = \underbrace{\frac{1}{2\eta} - \frac{1}{2\eta^2}\langle\Delta y^2\rangle}_{\text{kinetic term}} + \underbrace{\frac{1}{2}\langle y^2\rangle}_{\text{potential term}} \tag{3.13}$$

where $\langle y^2\rangle$ is the Monte Carlo average of the average values of the set $\{y_j^2\}$ on many paths, and likewise $\langle\Delta y^2\rangle$ is the average of the average values of $\{y_{j+1} - y_j\}$.

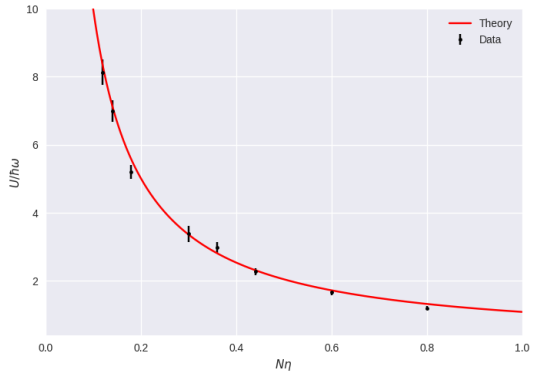

Figure 3.1: η is fixed at 0.01 and the measurements are taken for values of N between 10 and 80.

By the virial theorem, we expect the internal energy to be equally distributed between the kinetic and the potential energy, so that in units of $\hbar\omega$

$$\frac{1}{2}\langle y^2\rangle = \frac{U}{2} = \frac{1}{2}\left(\frac{1}{2} + \frac{1}{e^{N\eta}-1}\right). \tag{3.14}$$

Fixing $N\eta = \beta\omega$, we can therefore perform a fit for $\langle y^2\rangle$ using the model function $a + bx^2$ to check the quality of our simulation.

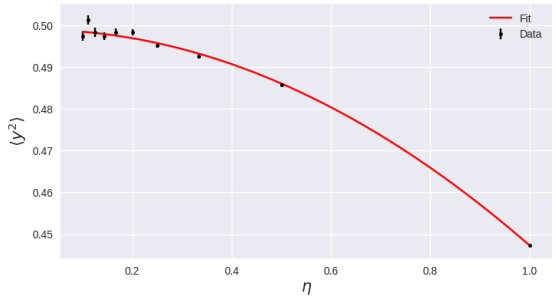

Figure 3.2: fitting with model function $a + bx^2$ at fixed $\beta\omega = 20$.

par	value	δ
a	0.49899	$\pm$0.00380
b	-0.05169	$\pm$0.00680

On the other hand, we may see that the term $\frac{1}{2\eta}$ that comes from the normalization constant $\mathcal{N} \propto \eta^{-N/2}$ is essential for the kinetic term to be both finite and positive in the continuum limit, which is obtained by letting $\eta \to 0$

while keeping $N\eta$ fixed. This is due to the fact that the free particle distribution $\exp(S^{\text{free}}_{E,L})$ is a Gaussian with variable $(\Delta y_j)^2$ and variance $\sigma^2 = 2\eta$, which implies

$$\frac{(\Delta y_j)^2}{\eta^2} \sim \frac{1}{\eta} \to_{\eta\to 0} +\infty. \tag{3.15}$$

Positivity is ensured by the caveat that the fluctuations Δy_j are milder than they would be if they were purely Gaussian, since there is the additional constraint $\sum_j \Delta y_j = 0$ due to the required closedness of the paths.

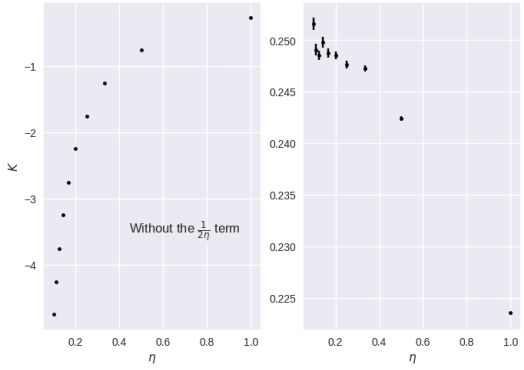

Figure 3.3: kinetic term with (right) and without (left) the $1/2\eta$ correction at $\beta\omega = 20$.

3.4 Correlation functions and energy splittings

The two-point connected correlation function of a hermitian operator $A = A(\hat{x})$ is defined as the mean value

$$C_2(\hat{A}, \tau) := \langle \hat{A}(\tau)\hat{A}(0)\rangle_C = \langle \hat{A}(\tau)\hat{A}(0)\rangle - \langle \hat{A}\rangle^2, \tag{3.16}$$

where $A(\tau)$ is the Euclidean-time evolved operator in a Heisenberg-like picture $\hat{A}(\tau) = e^{\hat{H}\tau/\hbar}\hat{A}e^{-\hat{H}\tau/\hbar}$.

In the $T \to 0$ limit, the correlation function can be written as the sum

$$C_2(\hat{A}, \tau) = \sum_n e^{-(E_n - E_0)\tau/\hbar} |\langle n|\hat{A}|0\rangle|^2 \tag{3.17}$$

and for large values of τ the most relevant contribution is given by the term $n = \bar{n}$ with the lowest energy that is connected to the empty state by $\hat{A}$. For instance, if $\hat{A} = \hat{x}$, then since $\hat{x} \sim \hat{a} + \hat{a}^\dagger$ the state $|\bar{n}\rangle$ is the first excited state, while if $\hat{A} = \hat{x}^2$ then $|\bar{n}\rangle$ corresponds to the second excited state. Since $|\langle 1|\hat{x}|0\rangle|^2, |\langle 2|\hat{x}^2|0\rangle|^2$ are constant, we can fit the exponentials to find the energy

splittings $E_1 - E_0$, $E_2 - E_0$ between the ground state and the first two excited ones.

In the discretized picture of our simulation, we use the variables y_j and compute

$$\langle y_{j+k} y_j \rangle_C \approx e^{-\Delta E_1 \tau/\hbar}, \quad \langle y_{j+k}^2 y_j^2 \rangle_C \approx e^{-\Delta E_2 \tau/\hbar} \tag{3.18}$$

for large $k = \tau/\delta\tau$. We notice that characteristic lengths of the correlations

$$\xi_1 = \hbar/\Delta E_1 \delta\tau, \quad \xi_2 = \hbar/\Delta E_2 \delta\tau \tag{3.19}$$

diverge for $\delta\tau \to 0$, which suggests the existence of a critical point at $\eta = 0$ (although there cannot be a phase transition in the 1D system) where both ξ_1, ξ_2 diverge as η^{-1}.

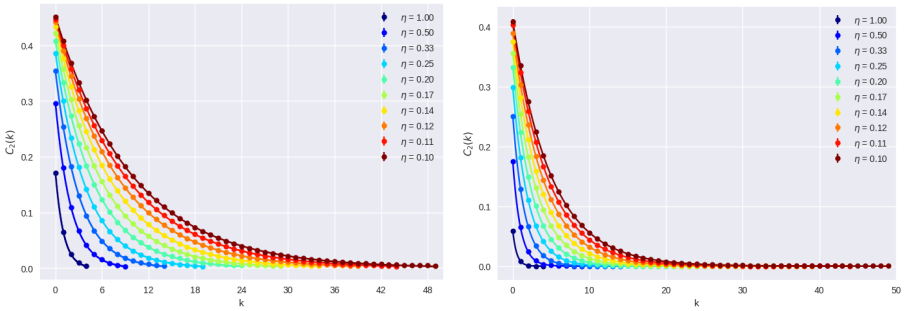

Figure 3.4: Correlation functions at fixed $\beta\omega = 20$ for y (left) and y^2 (right); as η becomes smaller, $C_2(k)$ takes a longer and longer time to reach zero. Furthermore, the higher power of y converges significantly faster to zero for all values of η.

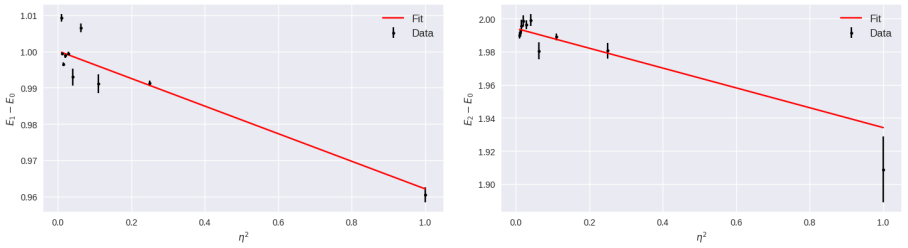

Figure 3.5: fitting with model function $ax + b$ at fixed $\beta\omega = 20$.

par	value	δ
a	-0.03809	± 0.00869
b	1.00017	± 0.00108

par	value	δ
a	-0.05999	± 0.02025
b	1.99410	± 0.00165

3.5 Ground state wavefunction

Introducing the characteristic function

$$\chi(x, x_a, x_b) = \begin{cases} 1 & \text{if } x_a < x < x_b, \\ 0 & \text{otherwise} \end{cases} \tag{3.20}$$

it is possible to compute the probability after a measurement of $\hat{x}$ to obtain x in the interval $[x_A, x_B]$ at temperature T as the average

$$P = \frac{1}{Z}\text{tr}\left[e^{-\beta H}\chi(x, x_A, x_B)\right]. \tag{3.21}$$

More explicitly, we get

$$P = \frac{1}{Z}\sum_n e^{-\beta E_n}\langle n|\chi(x; x_A, x_B)|n\rangle = \int_{x_a}^{x_b} |\psi_n(x)|^2 \, dx$$

which in the limit $T \to 0$ reduces to the ground state wavefunction. Thus, the histogram of the path values computed during our simulation should have the same Gaussian distribution as the theoretical wavefunction $\psi_0(x) = \frac{1}{\pi^{1/4}}e^{-x^2/2}$.

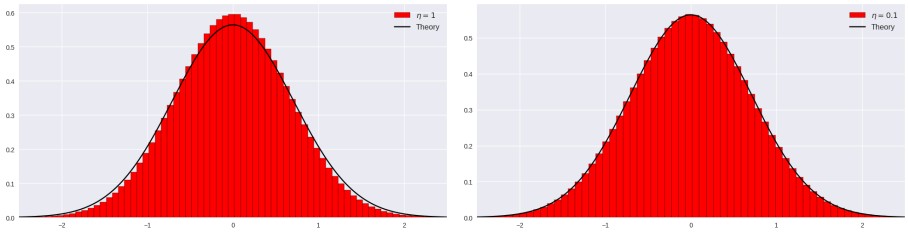

Figure 3.6: $\beta\omega = 20$; as η becomes smaller, the data fits better the theoretical curve.